Electronic Supplementary Material (ESI) for Journal of Materials Chemistry A.

Supporting Information

Adsorptive molecular sieving of aromatic over cyclic aliphatic hydrocarbons via the intrinsic/extrinsic approach

Gengwu Zhang,[a,‡] Xuanfu Zhu,[a,‡] Lukman O. Alimi,[a] Xin Liu,[a] Aiping Chen,[b] Basem M. Moosa[a] and Niveen M. Khashab[a,*]

[a]Smart Hybrid Materials Laboratory (SHMs), Advanced Membranes and Porous Materials Center (AMPMC), King Abdullah University of Science and Technology (KAUST), Thuwal, 23955-6900, Saudi Arabia

[b]Clean Combustion Research Center (CCRC), King Abdullah University of Science and Technology (KAUST), Thuwal 23955-6900, Saudi Arabia

‡These authors contributed equally.

*Corresponding Author. Email: niveen.khashab@kaust.edu.sa

1. Materials and methods

Materials. All reagents were commercially available and used as supplied without further purification.

Synthesis of TI and TA. TI[S1] and **TA**[S2] were synthesized according to previous literature reports, giving **TI** in 80.0% yield and **TA** in 96.5% yield. The obtained **TI** and **TA** were recrystallized from ethyl acetate solution and dried under vacuum for one day.

Materials Activation. The activated **TI** or **TA** crystals were prepared under vacuum at 90 °C for 12 h to remove the residual solvent molecules. The activated **TI** or **TA** after adsorption can be regenerated by heating at 9 0°C for 12 h under vacuum.

Single-Crystal Growth. Single crystals of **TI** with toluene (**Tol**): 10 mg of activated **TI** was dissolved in 1.5 ml of **Tol**, the crystal can be obtained by slow evaporation at room temperature for 72 h.

Single crystals of **TA** with **Tol**: 10 mg of activated **TA** was dissolved in 1.5 ml of **Tol**, the crystal can be obtained by slow evaporation at room temperature for 72 h.

Crystallization of **TI** with methylcyclohexane (**MCH**): 10 mg of activated **TI** was dissolved in 1.5 ml of different organic solvents. The solution was added to 0.1 ml of **MCH** for slow evaporation or diffusion with **MCH** at room temperature. White powder was obtained after several days (Table S2).

Crystallization of **TA** with **MCH**: 10 mg of activated **TA** was dissolved in 1.5 ml of different organic solvents. The solution was added to 0.1 ml of **MCH** for slow evaporation or diffusion with **MCH** at room temperature. White powder was obtained after several days (Table S2).

Solid-Vapor Sorption Experiments. Single component sorption: An open 5

ml vial containing 30 mg of **TI** or **TA** was placed in a sealed 20 ml vial containing 1.5 ml of guest solvent at room temperature.

Mix component sorption: An open 5 ml vial containing 30 mg of **TI** or **TA** was placed in a sealed 20 ml vial containing an equimolar mixture of **Tol/MCH**.

For both single and mixed component sorption experiment, the uptake capacity of **TI** or **TA** was measured at different time intervals by completely dissolving the samples in $CDCl_3$ for ^1H NMR, and the value was determined from the ratio of guest and host peaks.

NMR experiment. NMR spectra were recorded on Bruker-500 (500MHz for ^1H; 126 MHz for ^{13}C) instruments.

Thermogravimetric analysis. Thermogravimetric analysis (TGA) was carried out using a TGA Discovery 5500 with an automated vertical overhead thermobalance. The samples were heated at 10 °C/min from 25 °C to 800 °C using N_2 as the protective gas.

Powder X-ray diffraction. Powder X-ray diffraction (PXRD) data were collected using a Bruker D8 Advance X-ray diffractometer (40 kV, 40 mA) with the Cu Kα radiation (λ = 1.54178 Å). 2θ scans were performed in the range of 3.0−50° with a increment of 0.0197144° at a scan speed of 4.9286 (°/min). The sample was placed in a zero-background sample holder.

Nitrogen Adsorption Experiment. Low-pressure gas adsorption measurement was performed on a Micromeritics Accelerated Surface Area and Porosimetry System (ASAP) 2020 surface area analyzer. Samples were degassed under dynamic vacuum for 12 h at 90 °C prior to each measurement. N2 isotherms were measured using a liquid nitrogen bath (77 K).

Single crystal X-ray diffraction. Single crystal X-ray diffraction data were collected by a Bruker D8 Venture equipped with a digital camera diffractometer using graphite-monochromated Mo Kα radiation (λ= 0.71073 Å) or Cu Kα (λ=

1.54178 Å). Data reductions were carried out by a standard procedure using the Bruker software package SaintPlus 6.01.[S3] The absorption and other systematic errors corrections were performed by SADABS.[S4] The structures were solved by direct methods using SHELXS-2008 and refined using SHELXL-2018.[S5] X-Seed[S6] was used as the graphical interface for the SHELX program suite. Data collection, structure refinement parameters and crystallographic data for the crystals are given in Table S1.

Gas chromatography (GC) analysis. GC measurements were carried out using an Agilent 7890A instrument configured with an FID detector and a HPINNOWAX column (60 m × 0.320 mm × 0.5 μm). The following GC method was used: the oven was programmed in 40 °C with 35 min hold; injection temperature was 180 °C; detector temperature was 250 °C with hydrogen, air, and make-up flow-rates of 40, 400, and 15 mL min^{-1}, respectively; helium (carrier gas) flowrate was 3.0 mL min^{-1}.

Solvent-accessible voids calculation. Solvent-accessible voids can be visualized by calculating Connolly surfaces using MS-ROLL,[S7,S8] another program incorporated into X-Seed.

Pore size distribution calculation. Molecular modelling of **TA** and **TI** were constructed by referring to their single crystal structures of Tol@TI and Tol@TA by removing the guest/solvent molecules. Zeo^{++} is used to analyze the pore size distribution.[S9]

2. Crystallography data

Table S1. Crystallographic details for **TI** and **TA** macrocycle with **Tol**.

IDENTIFICATION CODE	TA@Tol	TI@Tol
Empirical formula	$C_{52}H_{71}N_6$	$C_{49}H_{56}N_6$
Formula weight (g/mol)	777.94	728.99
Temperature /K	120.0	120.0
Crystal system	Orthorhombic	Monoclinic
Space group	$P2_12_12_1$	$P2_1$

***a*/ Å**	8.5912(4)	11.3748(6)
***b*/ Å**	34.7476(15)	10.4601(4)
***c*/ Å**	45.4824(19)	18.2806(9)
α/°	90	90
β/°	90	100.519(2)
γ/°	90	90
Volume/ Å^3	13577.6(10)	2138.50(18)
Z	12	2
ρcalcg/cm^3	1.142	1.132
F(000)	5008	784
Radiation	CuKα (λ = 1.54178)	MoKα (λ = 0.71073)
reflections collected	160479	12714
Independent reflections	23155(R_{int} = 0.0360)	7311(R_{int} = 0.0243)
Data/restraints/para meters	21285/0/1489	6571/1/497
Goodness-of-fit on F2	1.056	1.043
Final R indexes [I>=2σ (I)]	$R1$ = 0.0646, $wR2$ = 0.1708	$R1$ = 0.0396, $wR2$ = 0.0863
CCDC numbers	2287896	2287895

Table S2. Crystallization solvents and methods for **TI** and **TA** macrocycle with **MCH**.

Compounds	Solvents	Methods	Results
TI (10mg)	1.5 ml DCM + 0.1ml MCH	evaporation	powder
	1.5 ml $CHCl_3$ + 0.1ml MCH		powder
	1.5 ml Acetone + 0.1ml MCH		powder
	1.5 ml Ethyl acetate + 0.1ml MCH		powder
	3 ml CH_3CN + 0.1ml MCH		powder
	1.5 ml DCM + 1.5 ml MCH	diffusion	powder
	1.5 ml $CHCl_3$ + 1.5 ml MCH		powder
	1.5 ml Acetone + 1.5 ml MCH		powder
	1.5 ml Ethyl acetate + 1.5 ml MCH		powder
	3 ml CH_3CN + 1.5 ml MCH		powder
TA (10mg)	1.5 ml DCM + 0.1ml MCH	evaporation	powder
	1.5 ml $CHCl_3$ + 0.1ml MCH		powder
	1.5 ml Acetone + 0.1ml MCH		powder
	1.5 ml Ethyl acetate + 0.1ml MCH		powder
	1.5 ml MeOH + 0.1ml MCH		powder

	1.5 ml DCM + 1.5 ml MCH	diffusion	powder
	1.5 ml $CHCl_3$ + 1.5 ml MCH		powder
	1.5 ml Acetone + 1.5 ml MCH		powder
	1.5 ml Ethyl acetate + 1.5 ml MCH		powder
	1.5 ml MeOH + 1.5 ml MCH		powder

3. Supplementary figures

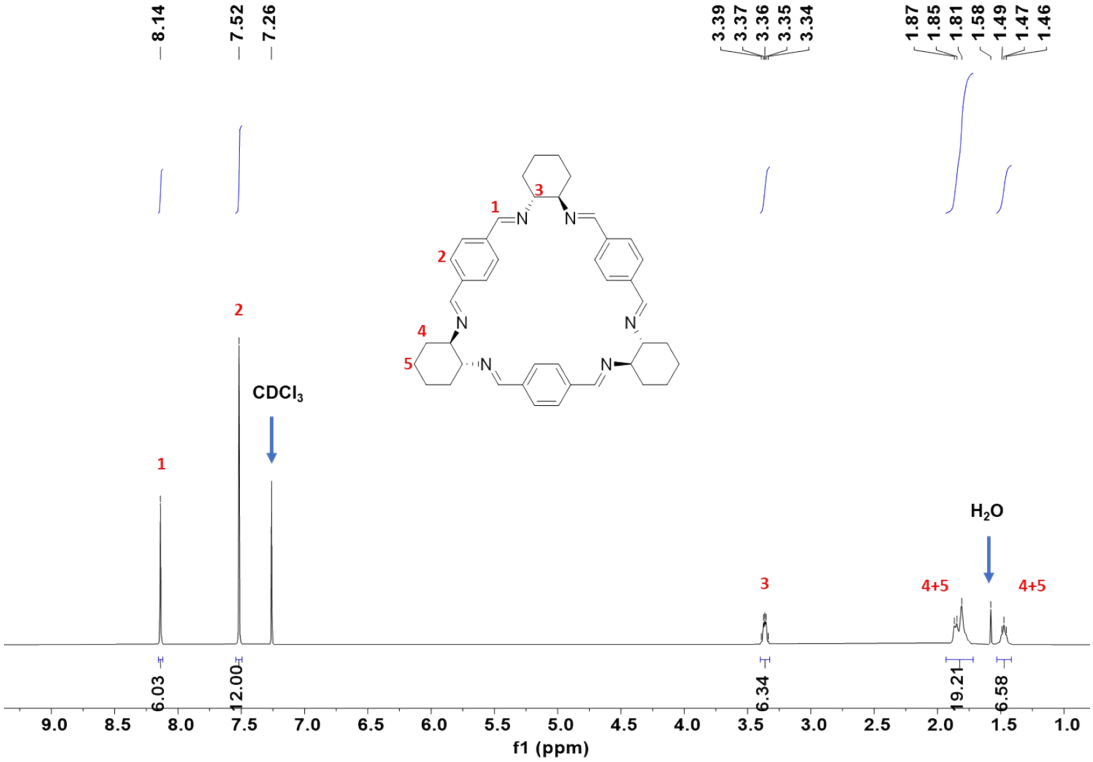

Figure S1. ^{1}H NMR spectrum (500 MHz, chloroform-*d*, 298K) of **TI**.

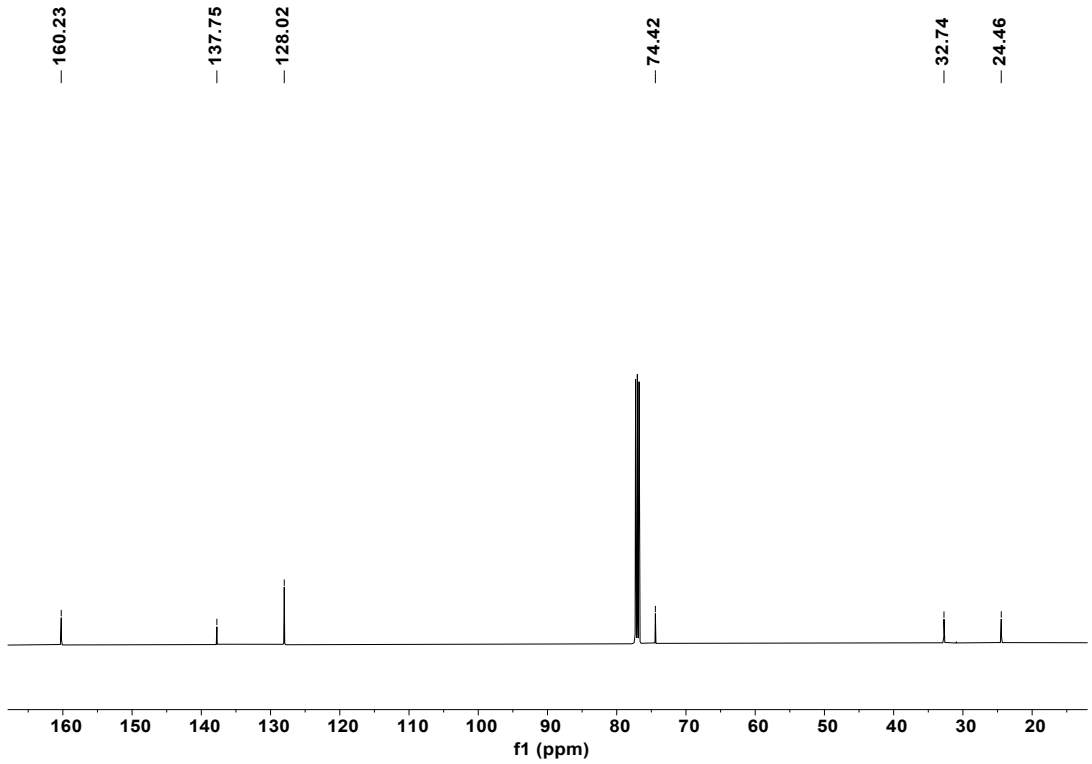

Figure S2. ^{13}C NMR spectrum (126 MHz, chloroform-*d*, 298K) of **TI**.

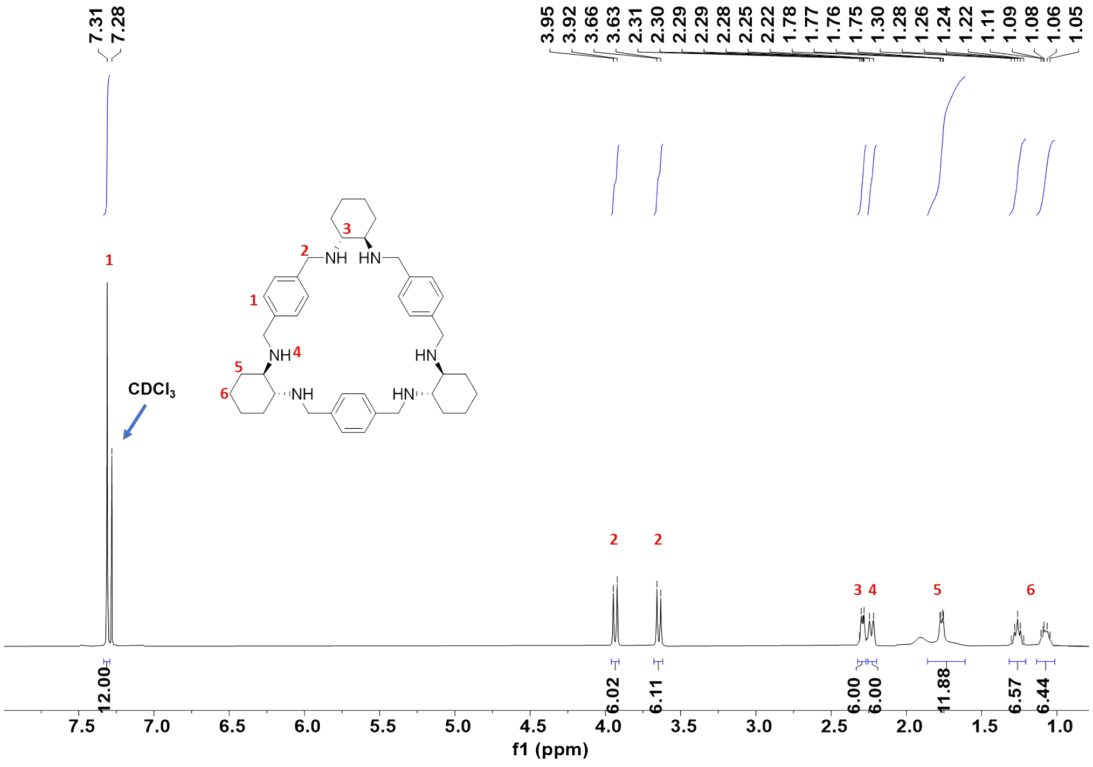

Figure S3. ^{1}H NMR spectrum (500 MHz, chloroform-*d*, 298K) of **TA**.

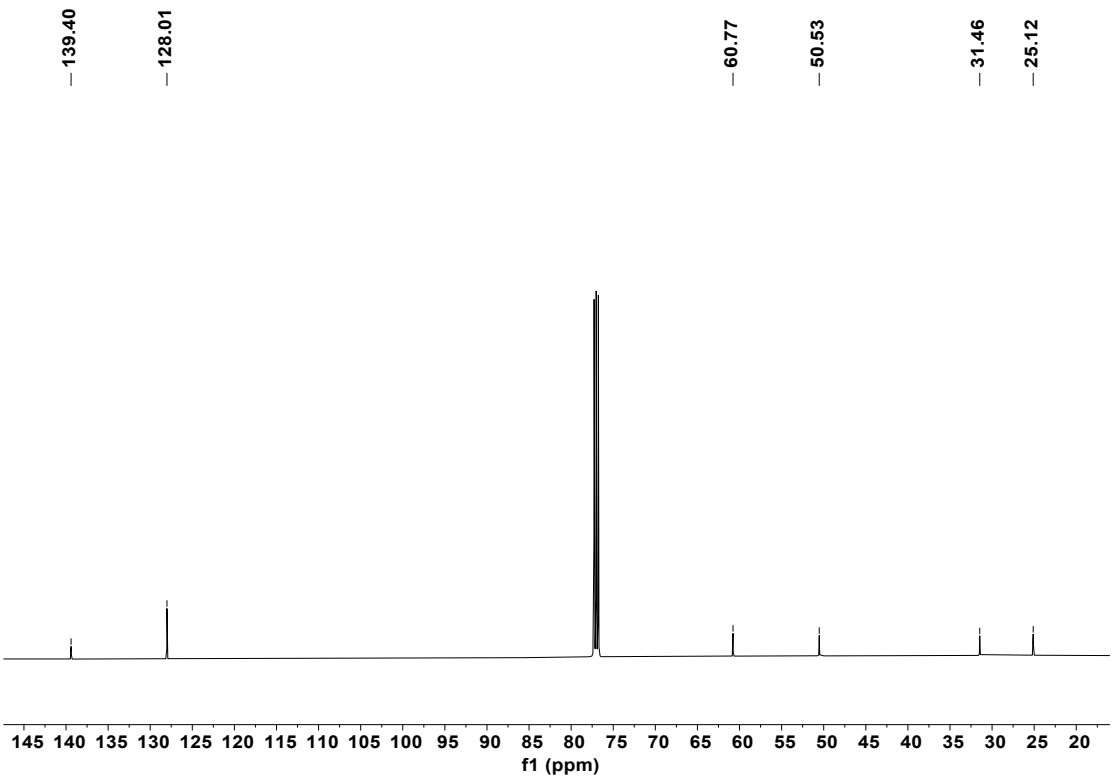

Figure S4. ^{13}C NMR spectrum (126 MHz, chloroform-*d*, 298K) of **TA**.

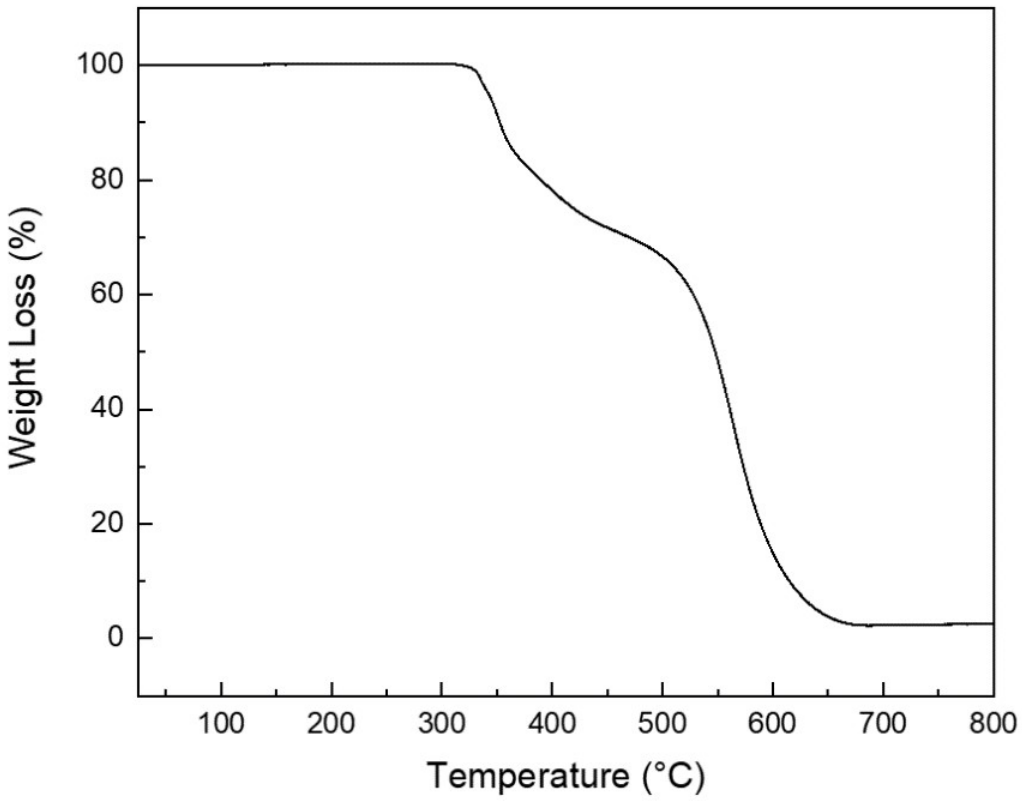

Figure S5. TGA curve of pure activated **TI**.

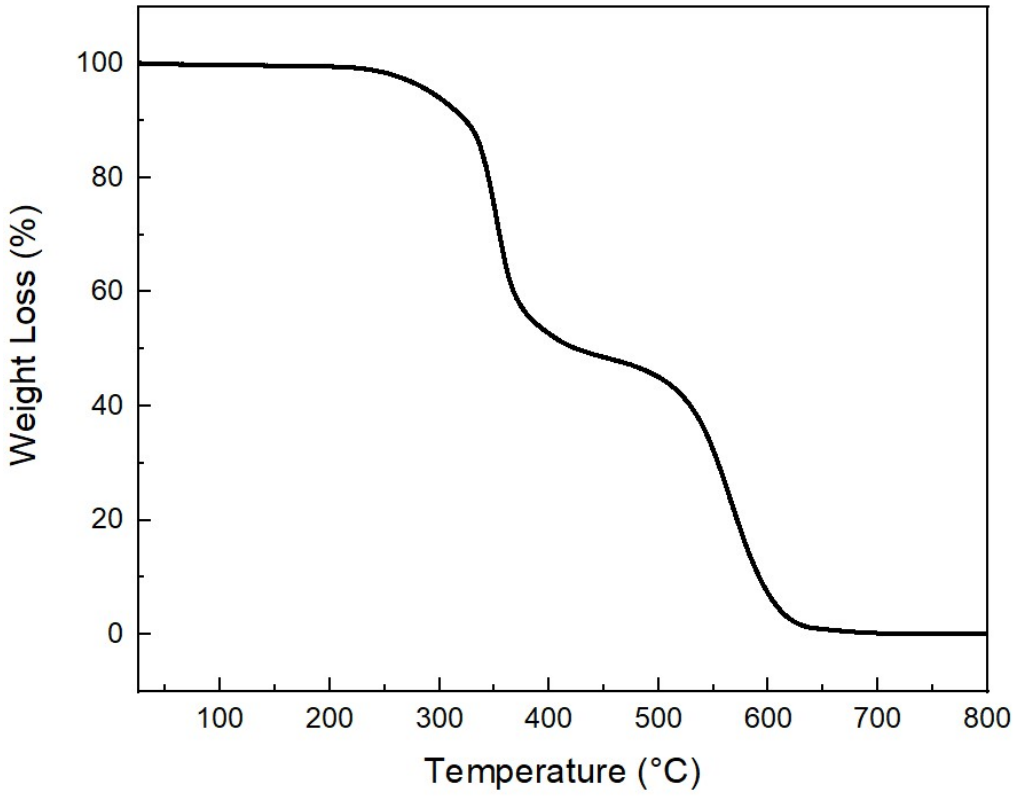

Figure S6. TGA curve of pure activated **TA**.

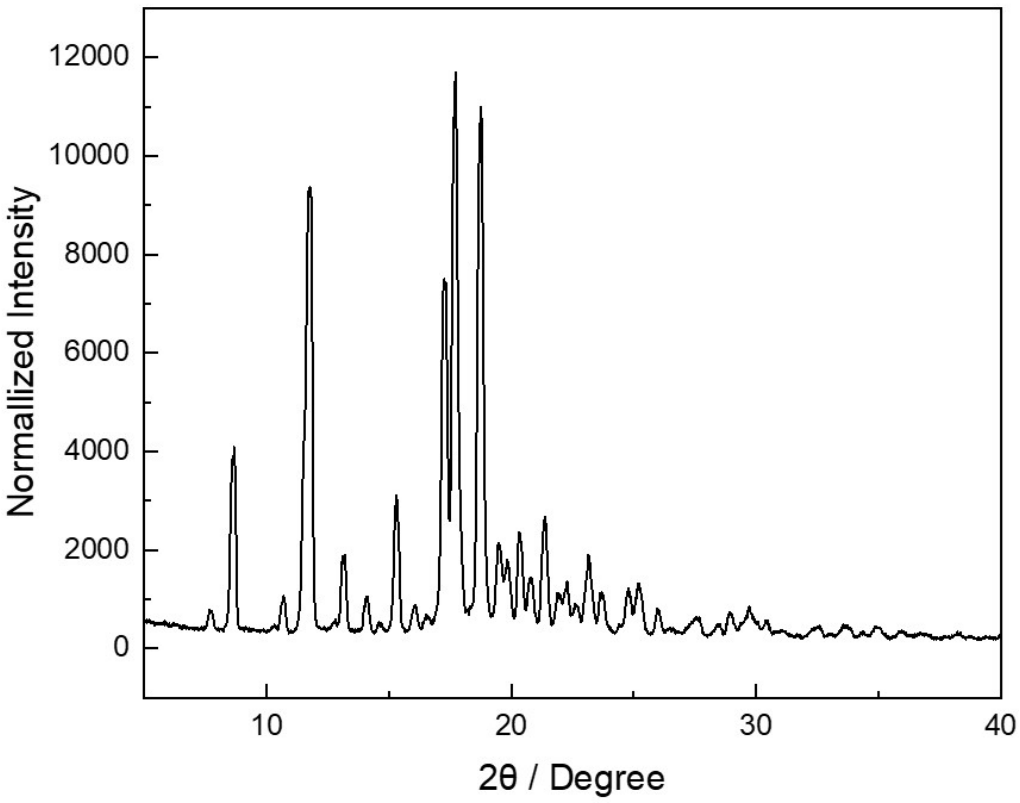

Figure S7. PXRD pattern of pure activated **TI**.

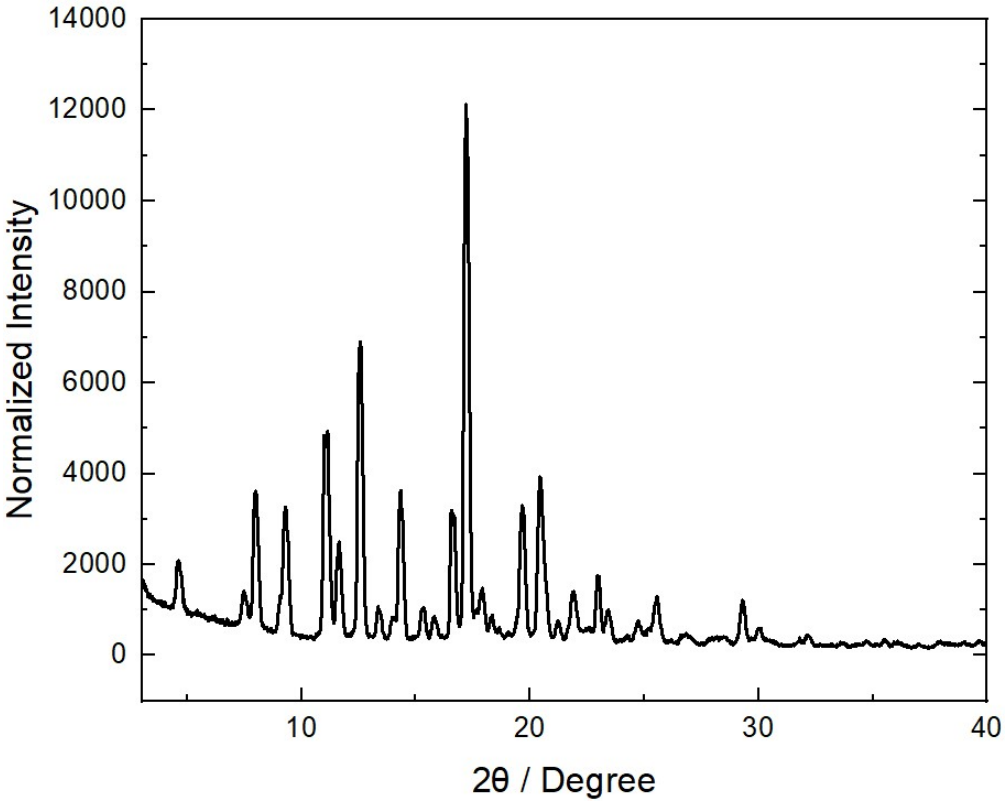

Figure S8. PXRD pattern of pure activated **TA**.

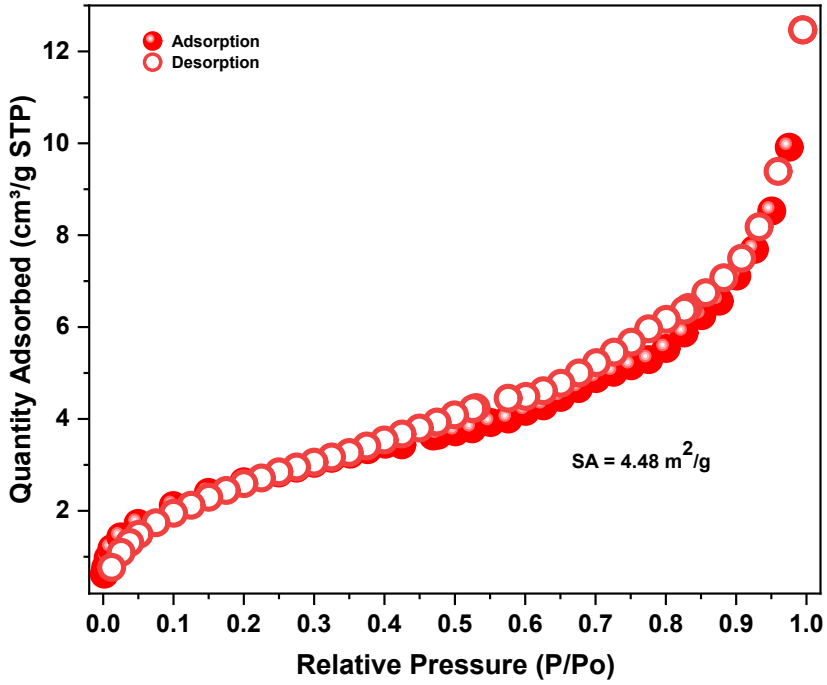

Figure S9. Nitrogen adsorption isotherm at 77 K for activated **TI**.

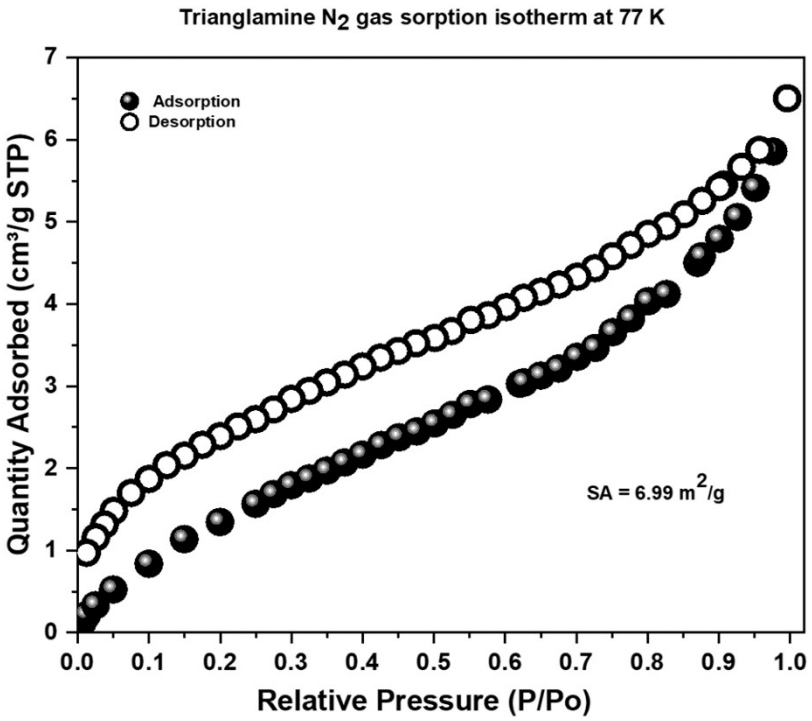

Figure S10. Nitrogen adsorption isotherm at 77 K for activated **TA**.

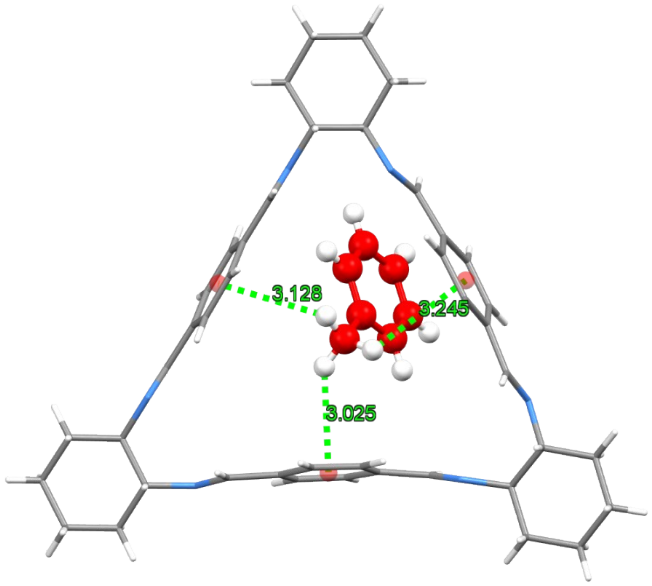

Figure S11. Asymmetric unit of **Tol@TI** showing C-H···π interactions between host **TI** macrocycle and guest **Tol**.

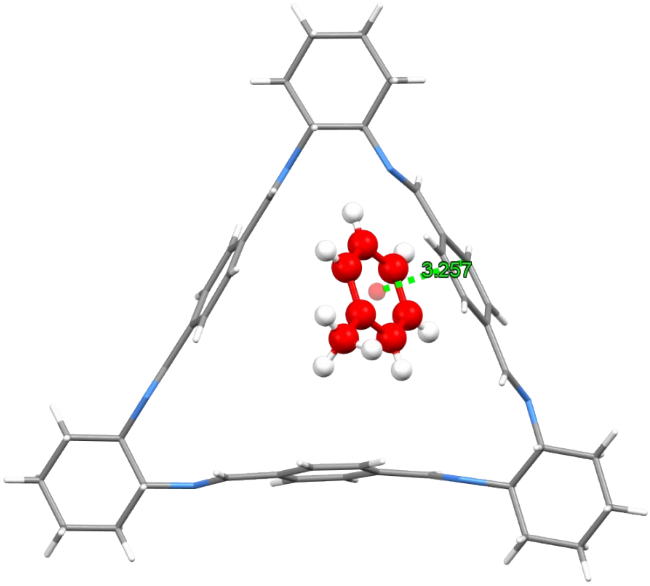

Figure S12. Asymmetric unit of **Tol@TI** showing π···π interaction between host **TI** macrocycle and guest **Tol**.

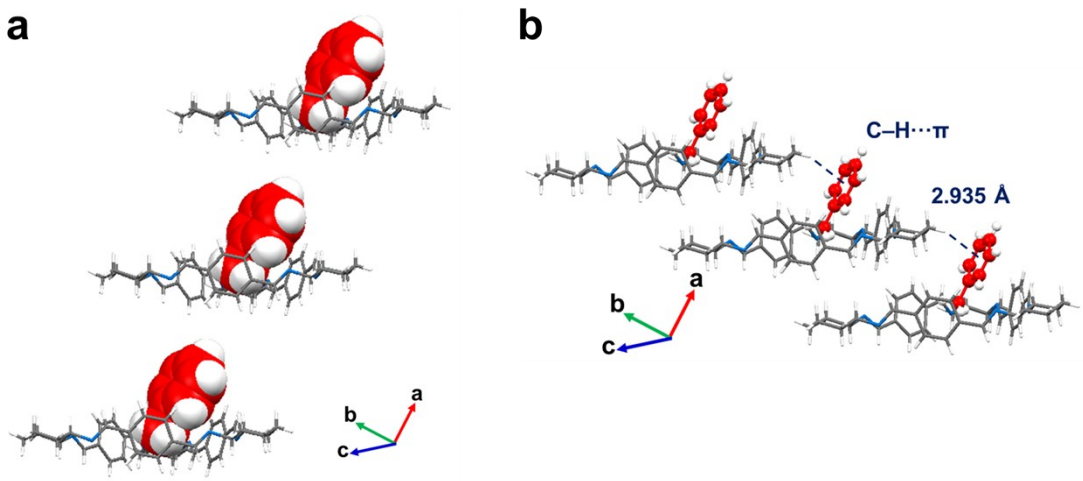

Figure S13. Perspective view showing inclined 1D packing arrangement of **Tol@TI** along crystallographic *a* axis and the C-H···π interaction between **Tol** and adjacent **TI**.

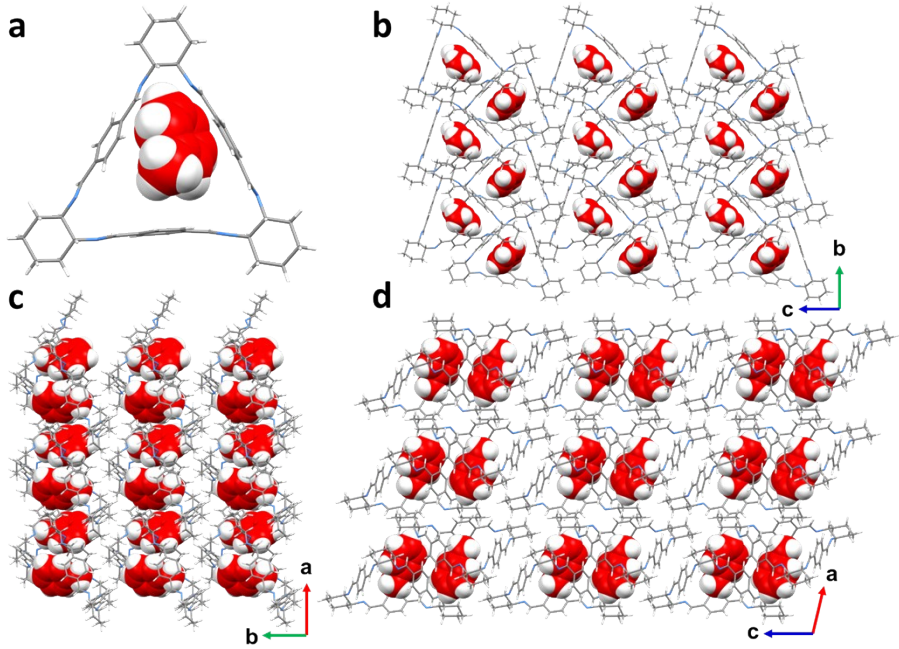

Figure S14. (a) Asymmetric unit of **TolI@TI**. (b-d)Packing arrangement of **TolI@TI** viewed from all crystallographic axes.

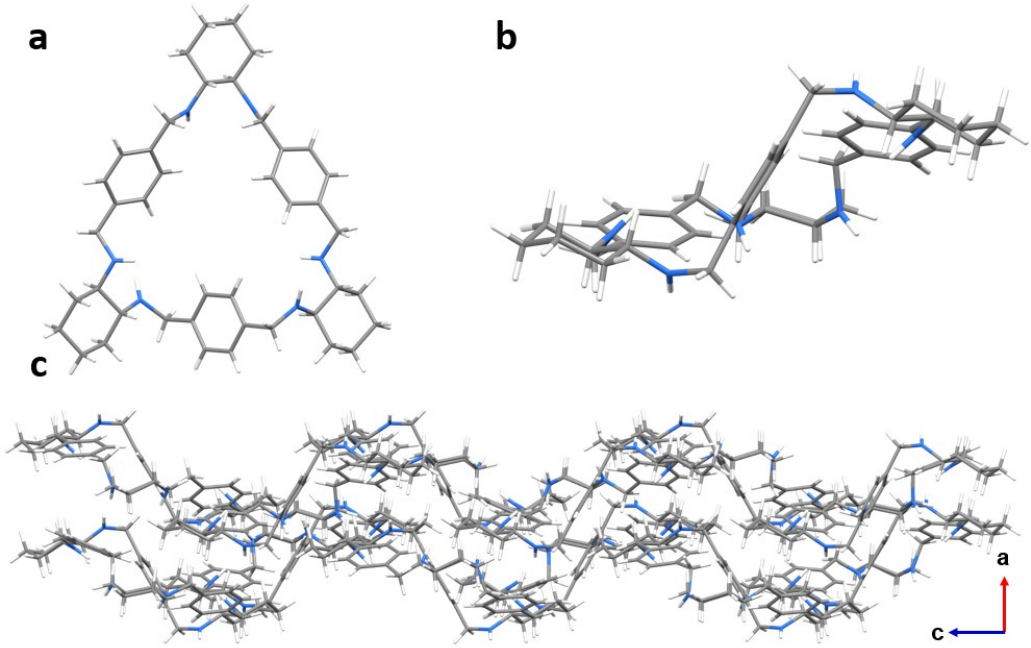

Figure S15. (a) Top view and (b) Side view of **TA** macrocycles in **TolI@TA**. (c) Packing arrangement of **TA** macrocycle showing zigzag structure (guest molecules were hidden for clarity).

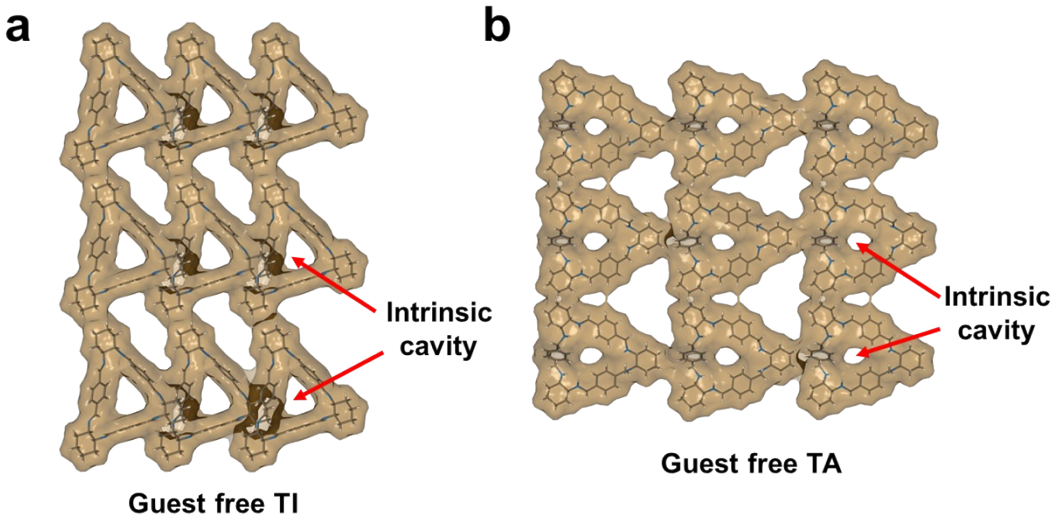

Figure S16. Single layer crystal packing structure along crystallographic a axis with the contact surfaces of (a) guest-free **TI** and (b) guest-free **TA** showing the guest accessible voids within their intrinsic cavities. The contact surfaces of empty **TI** and **TA** macrocycles were mapped using MSRoll program with probe radius of 1.2 Å. **TA** with distorted flexible conformation shows much smaller guest accessible voids than **TI**.

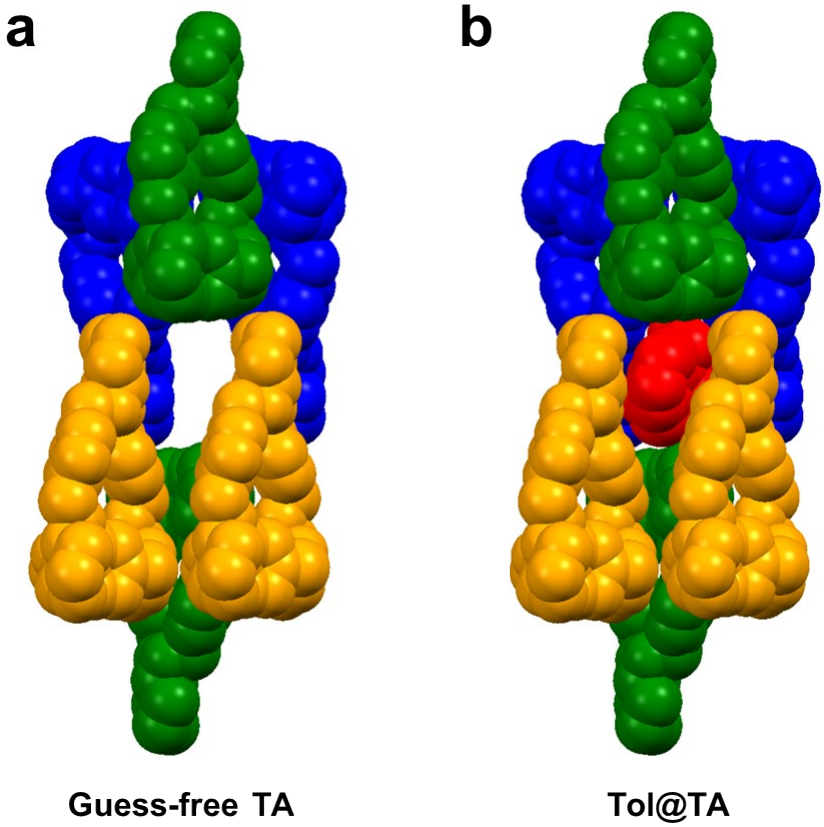

Figure S17. The 3D packing structure along crystallographic *c* axis of (a) guest-free **TA**

and (b) **Tol@TA**. The three **TI** host molecules in one asymmetric unit were colored in yellow, blue, and green, respectively. The guest **Tol** molecules were colored in red and located in the extrinsic channel.

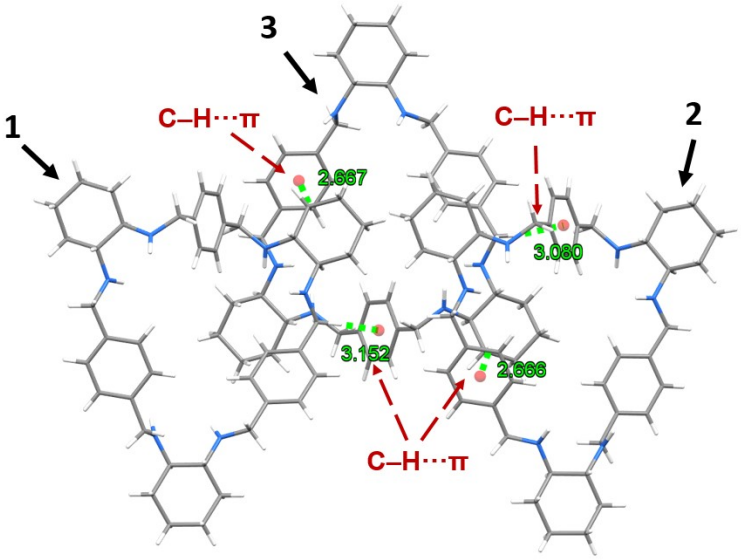

Figure S18. Perspective view showing some C-H···π interactions between **TA** macrocycle 1, 2 and 3.

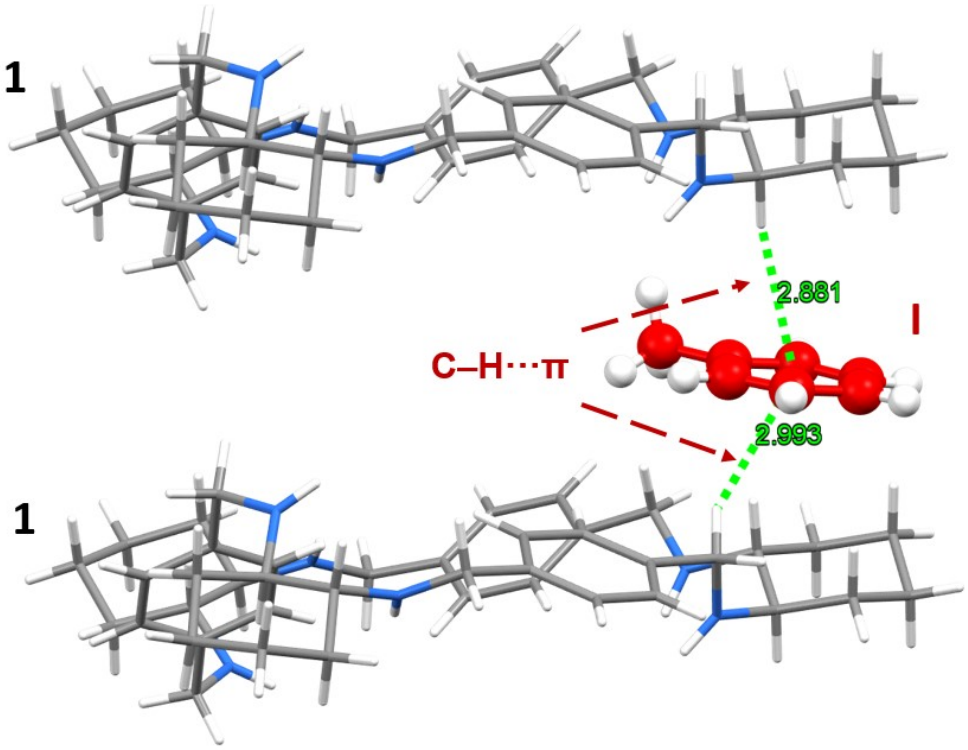

Figure S19. Perspective view showing some C-H···π interactions between **TA** macrocycle

1 and **Tol** I.

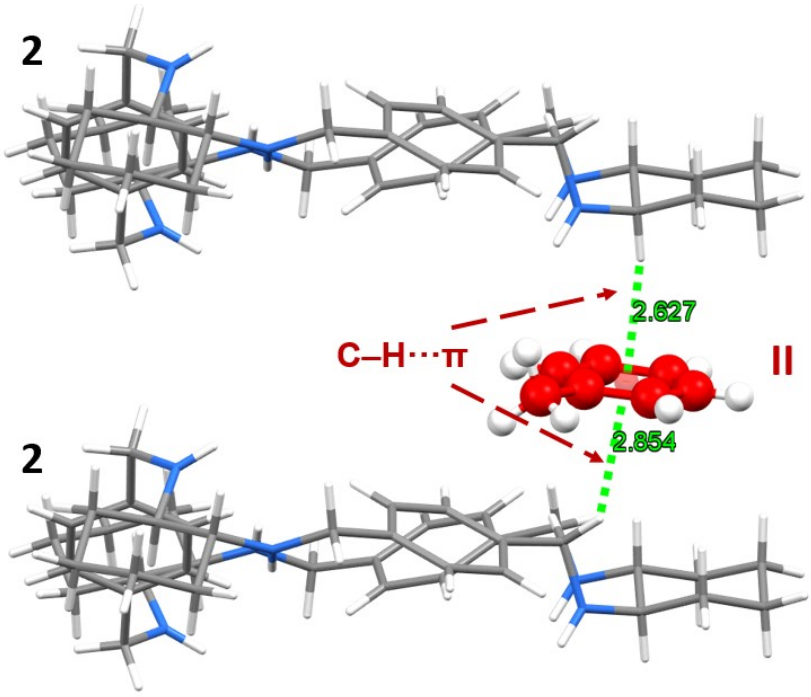

Figure S20. Perspective view showing some C-H···π interactions between **TA** macrocycle 2 and **Tol** II.

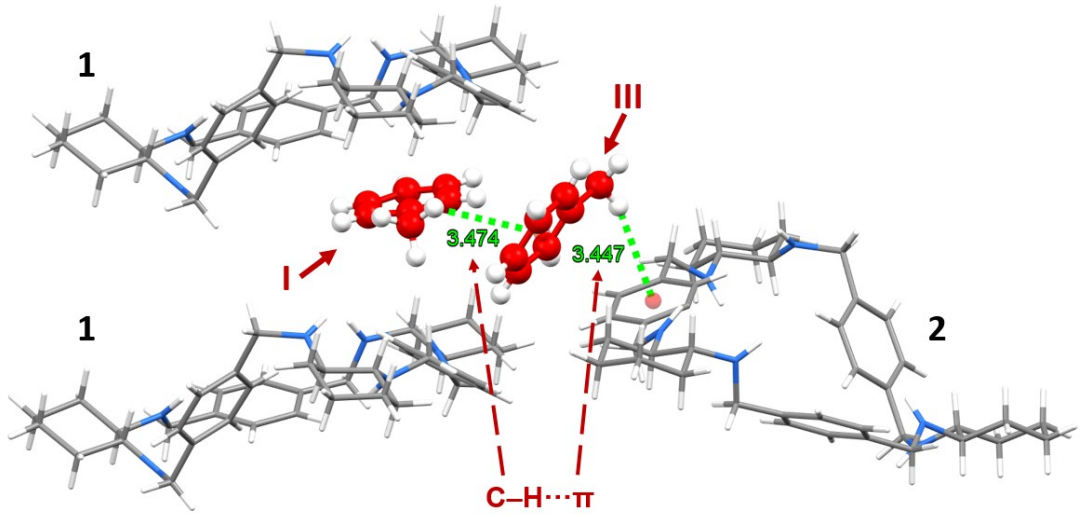

Figure S21. Perspective view showing some C-H···π interactions between **TA** macrocycle 1 and **Tol** I and III.

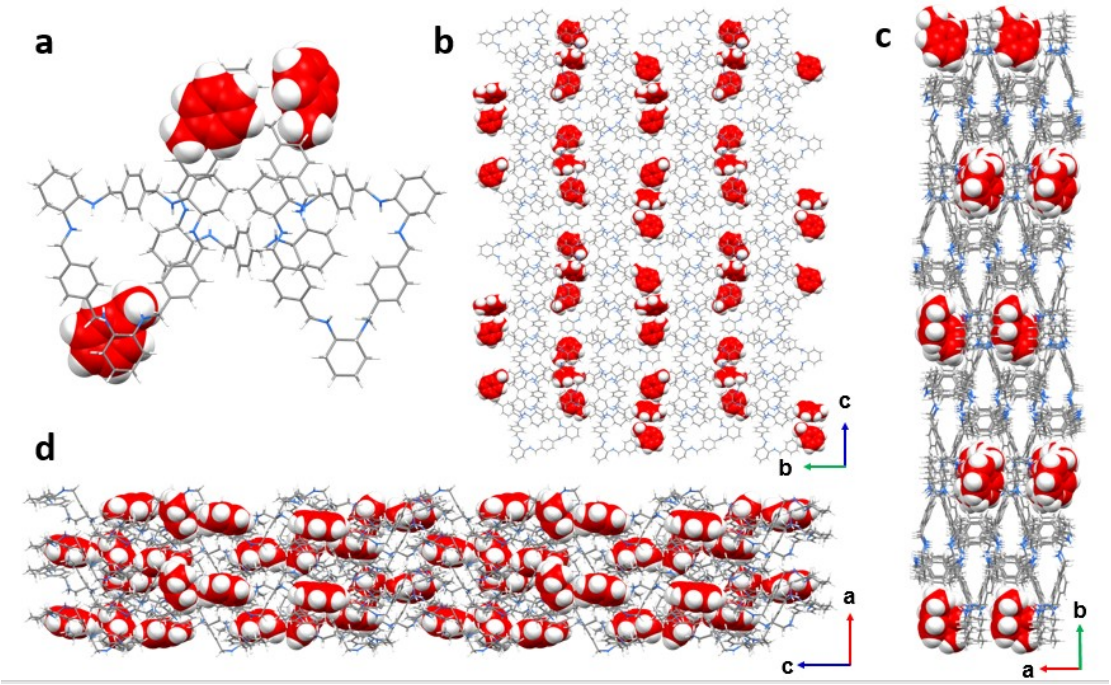

Figure S22. (a) Asymmetric unit of **Tol@TA**. (b-d) Packing arrangement of **Tol@TA** viewed from all crystallographic axes.

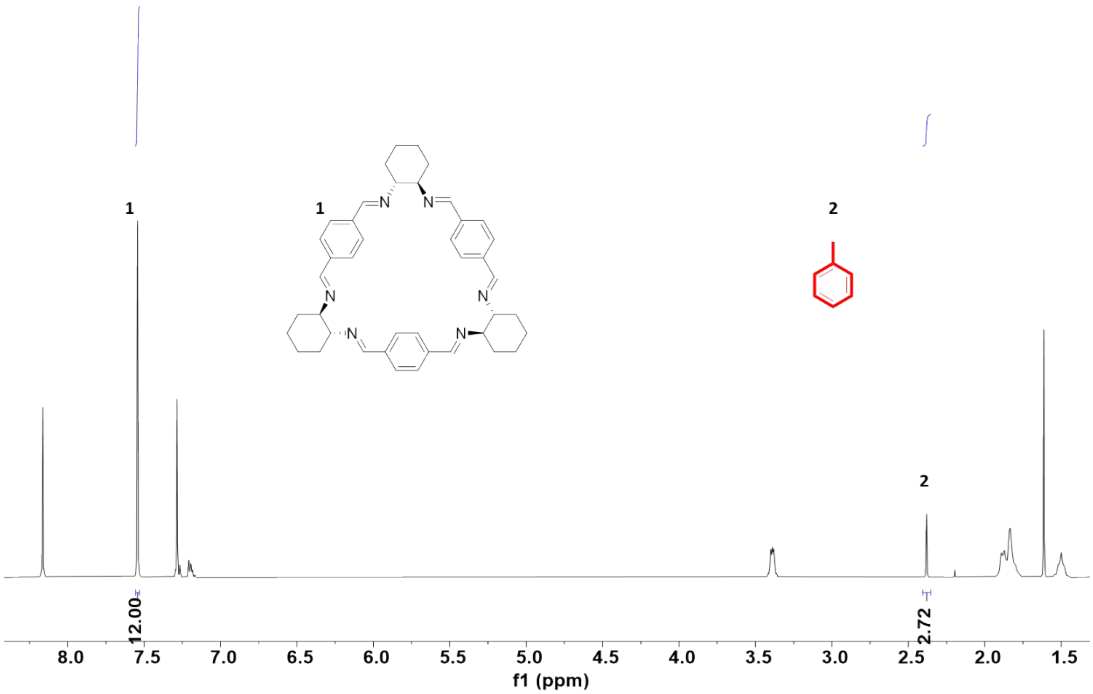

Figure S23. ^{1}H NMR spectrum (500 MHz, chloroform-*d*, 298K) of activated **TI** after absorption of **Tol** vapor until saturation. The integrations can be calculated as about 1.0 equiv. of **Tol** per **TI** molecule.

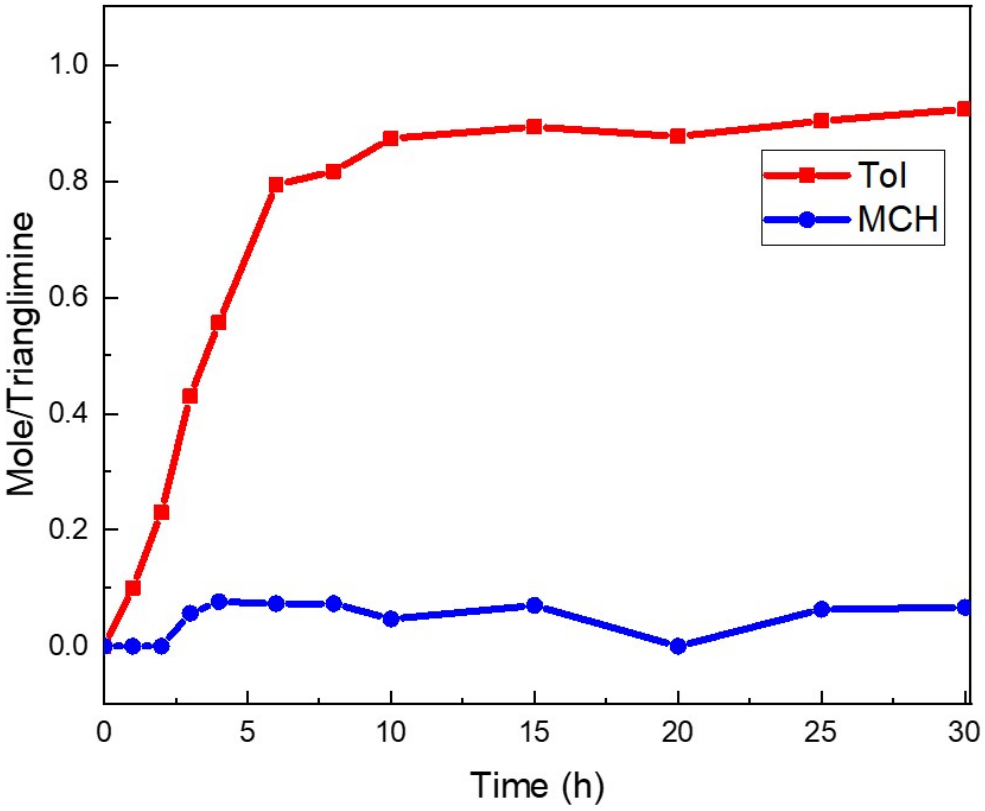

Figure S24. Time-dependent solid-vapor sorption curve of **TI** with single component of **Tol** and **MCH.**

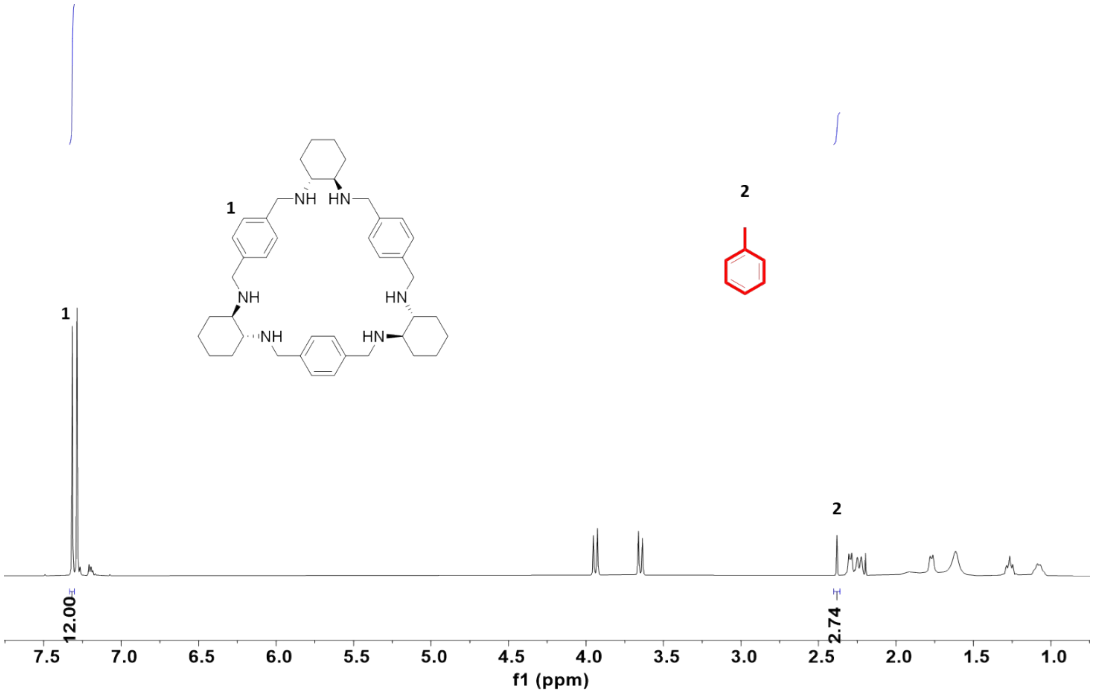

Figure S25. ^{1}H NMR spectrum (500 MHz, chloroform-*d*, 298K) of activated **TA** after absorption of **Tol** vapor until saturation. The integrations can be calculated as about 0.9 equiv. of **Tol** per **TA** molecule.

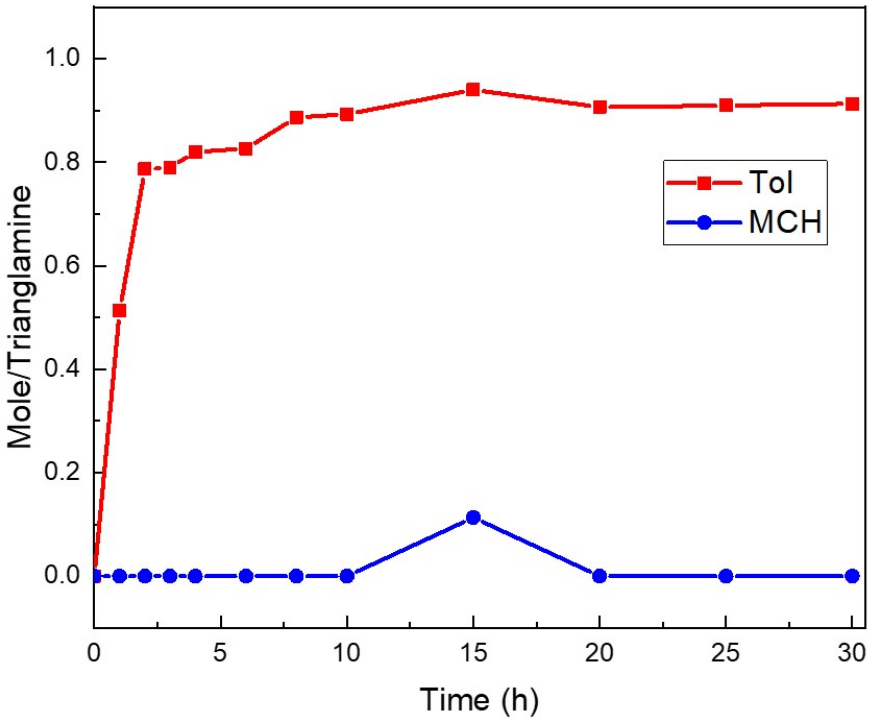

Figure S26. Time-dependent solid-vapor sorption curve of **TA** with single component of **Tol** and **MCH**.

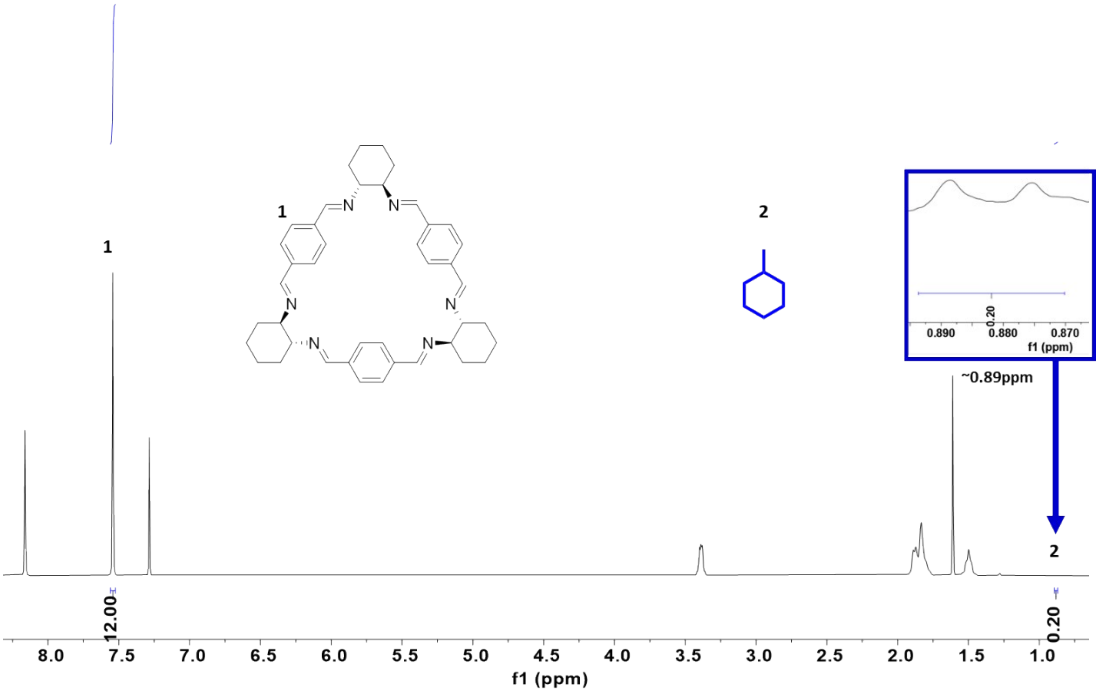

Figure S27. ^{1}H NMR spectrum (500 MHz, chloroform-*d*, 298K) of activated **TI** after absorption of **MCH** vapor until saturation. The integrations can be calculated as about 0.07 equiv. of **MCH** per **TI** molecule.

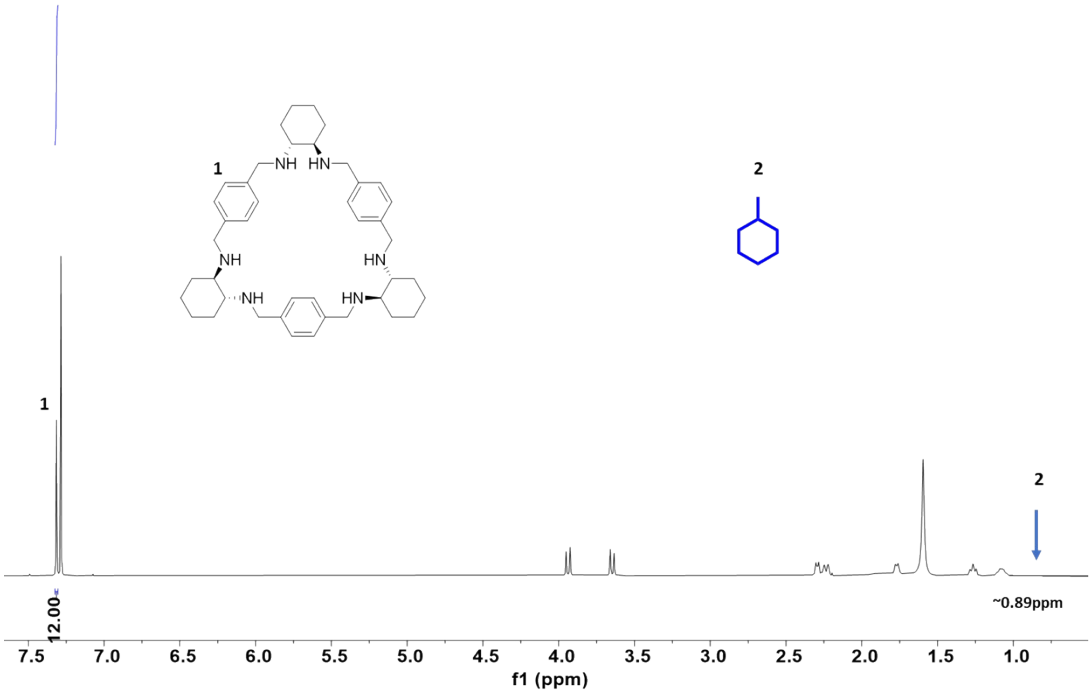

Figure S28. ^{1}H NMR spectrum (500 MHz, chloroform-*d*, 298K) of activated **TA** after absorption of **MCH** vapor until saturation.

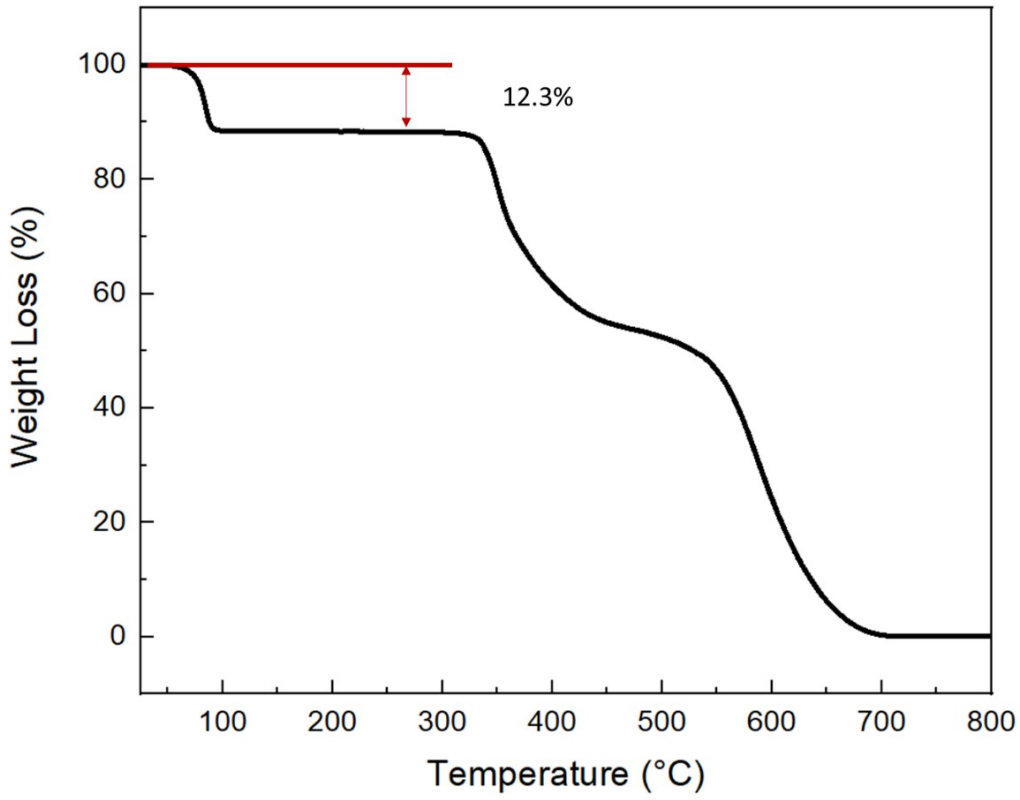

Figure S29. TGA curve of activated **TI** after absorption of **TOI** vapor until saturation.

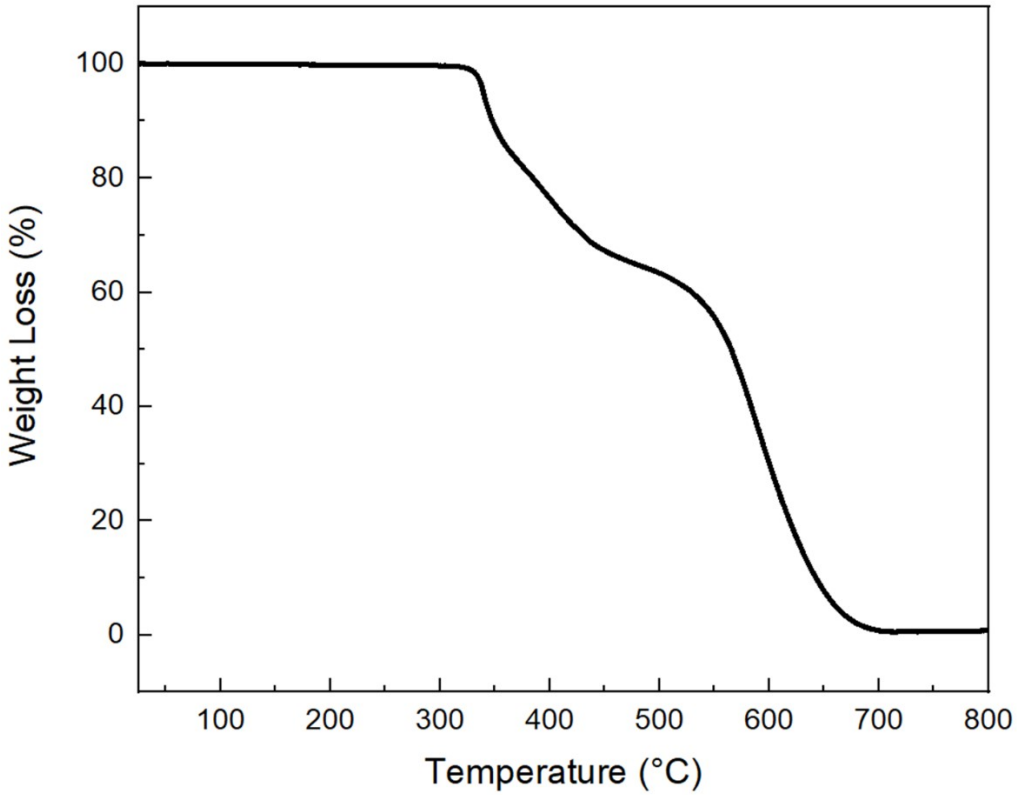

Figure S30. TGA curve of activated **TI** showing no absorption of **MCH** vapor upon exposure until saturation.

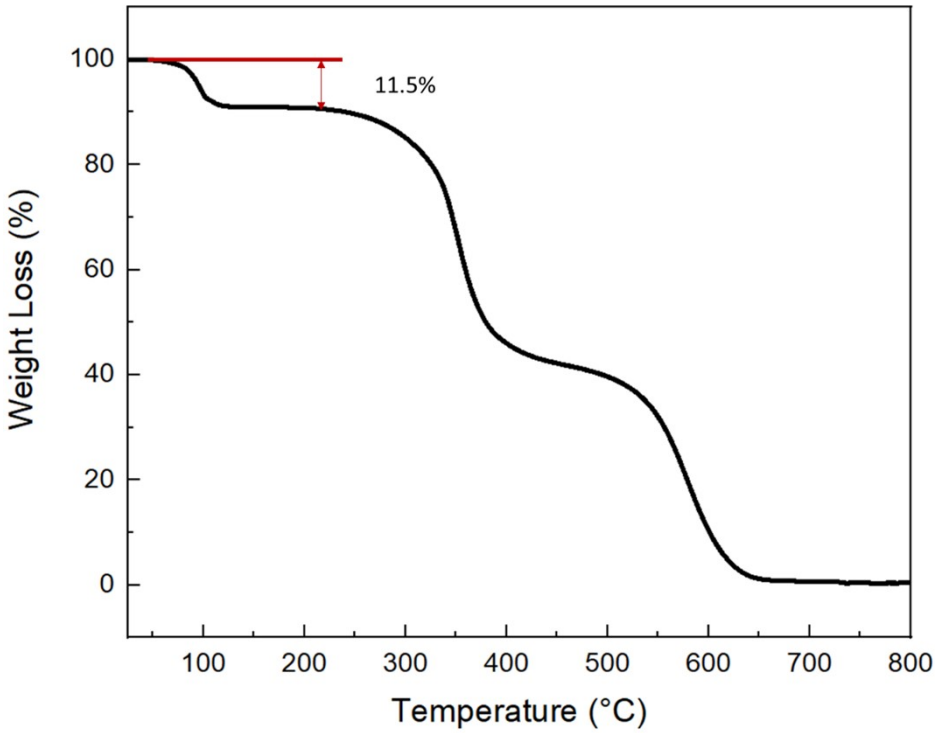

Figure S31. TGA curve of activated **TA** after absorption of **TOI** vapor until saturation.

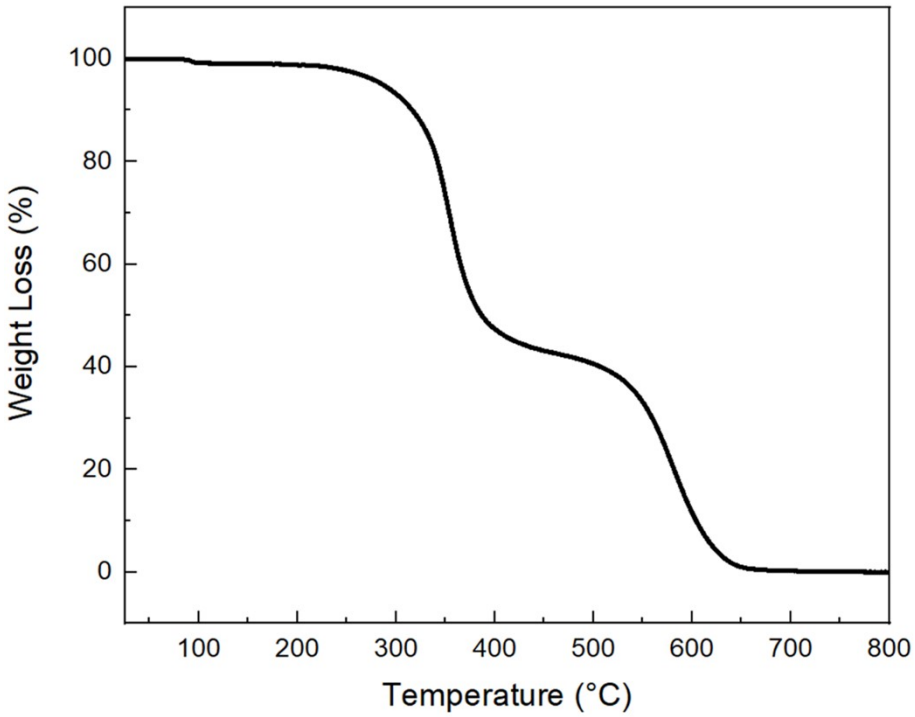

Figure S32. TGA curve of activated **TA** showing no absorption of **MCH** vapor upon exposure until saturation.

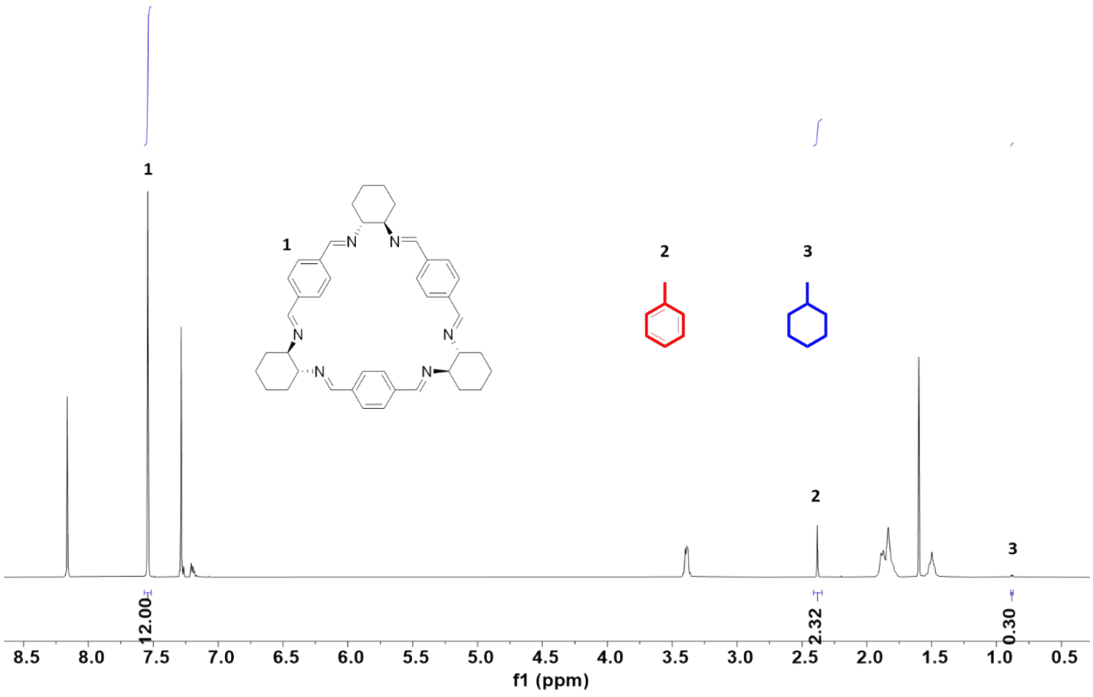

Figure S33. ^{1}H NMR spectrum (500 MHz, chloroform-*d*, 298K) of activated **TI** after exposure in the equal-volume **Tol/MCH** mixture until saturation.

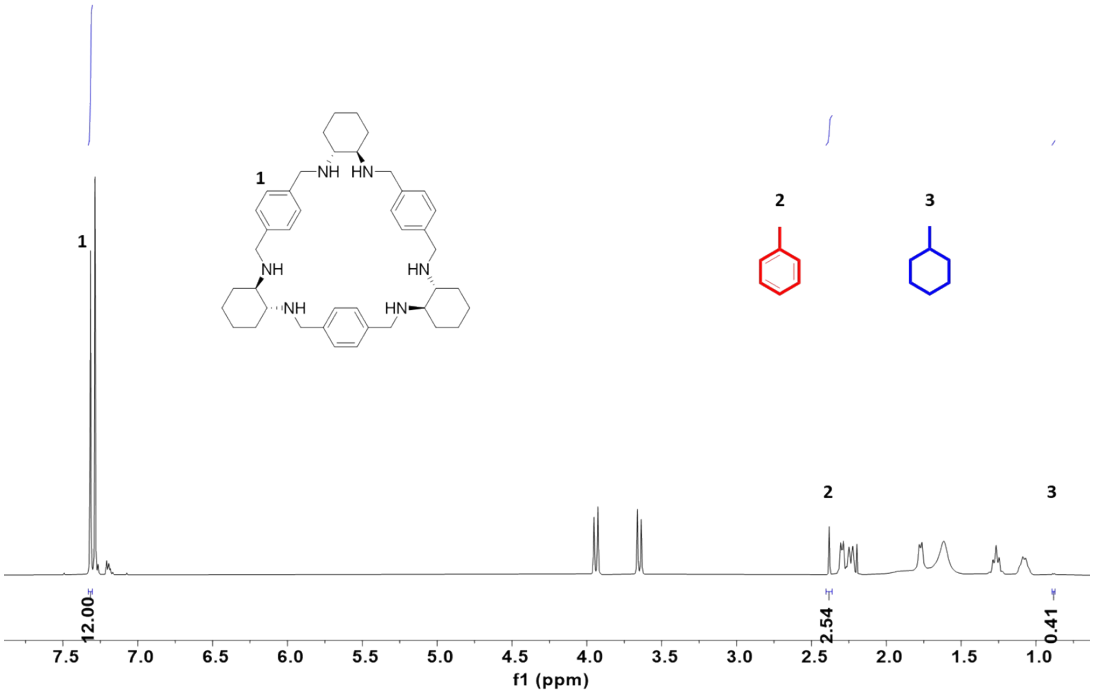

Figure S34. ^{1}H NMR spectrum (500 MHz, chloroform-*d*, 298K) of activated **TA** after exposure in the equal-volume **Tol/MCH** mixture until saturation.

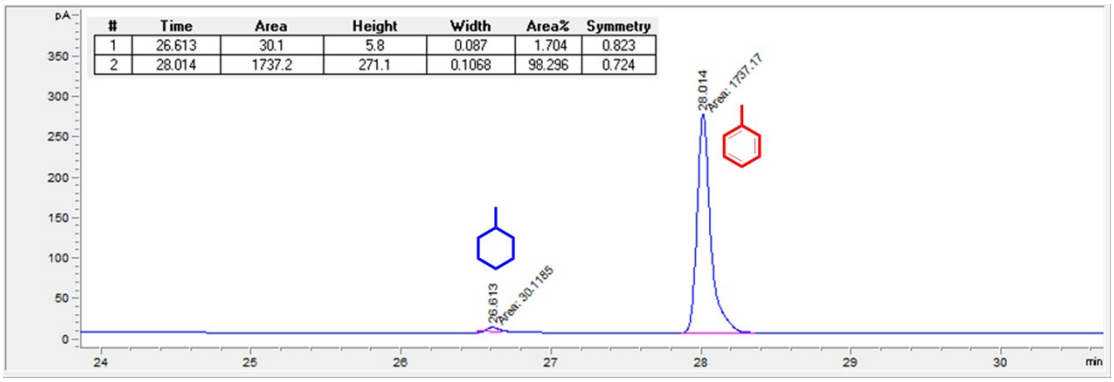

#	Time	Area	Height	Width	Area%	Symmetry
1	26.613	30.1	5.8	0.087	1.704	0.823
2	28.014	1737.2	271.1	0.1068	98.296	0.724

Figure S35. Relative uptakes of **Tol/MCH** adsorbed in **TI** after absorption of the equimolar mixture vapor until saturation using gas chromatography.

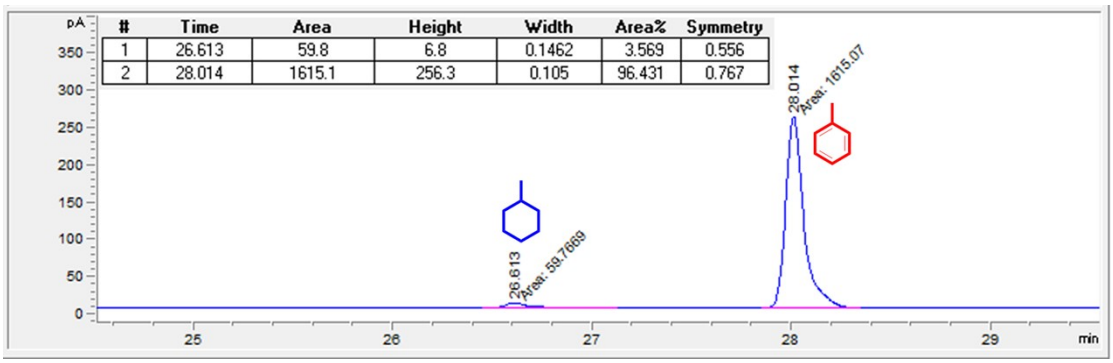

#	Time	Area	Height	Width	Area%	Symmetry
1	26.613	59.8	6.8	0.1462	3.569	0.556
2	28.014	1615.1	256.3	0.105	96.431	0.767

Figure S36. Relative uptakes of **Tol/MCH** adsorbed in **TA** after absorption of the equimolar

mixture vapor until saturation using gas chromatography.

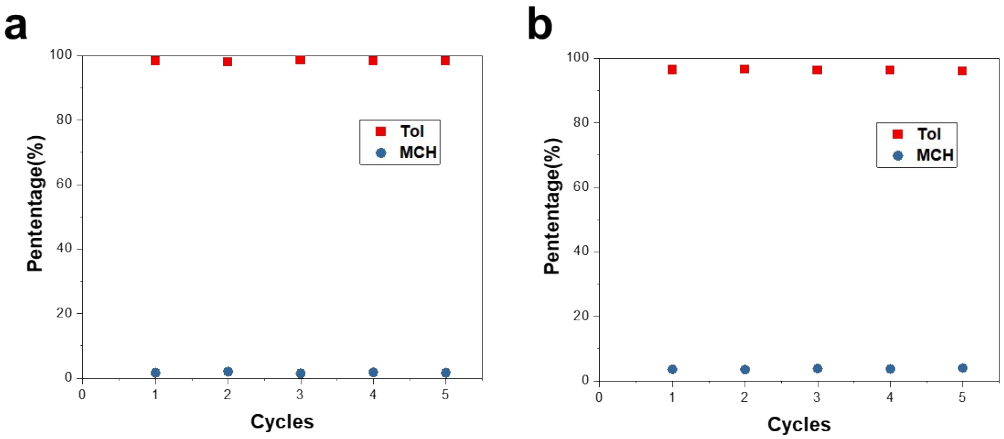

Figure S37. Relative uptakes of **Tol/MCH** adsorbed in (a) **TI** and (b) **TA** after absorption of the equimolar mixture vapor until saturation for five cycles.

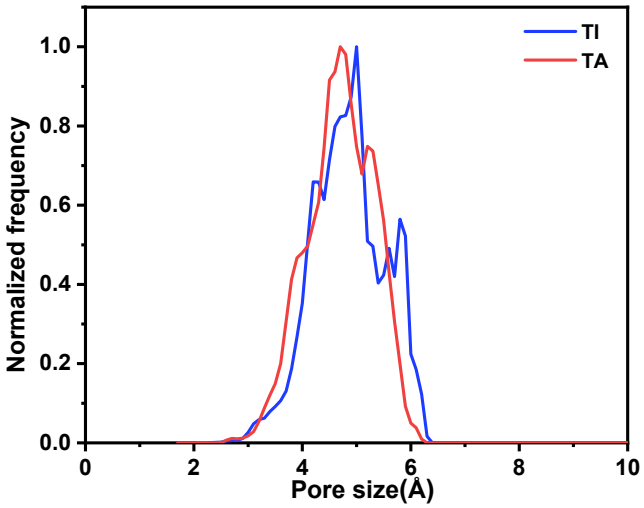

Figure S38. Simulated pore size distributions of the single crystal structures of **Tol@TI** and **Tol@TA** after removing **Tol** molecules.

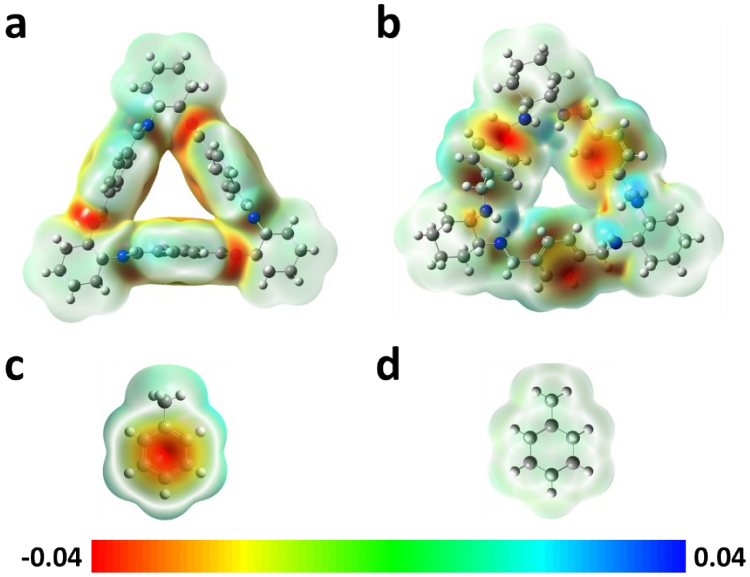

Figure S39. Electrostatic potentials (ESPs) mapped onto electron density isosurfaces of (a) **TI**, (b) **TA**, (c) **Tol**, and (d) **MCH**.

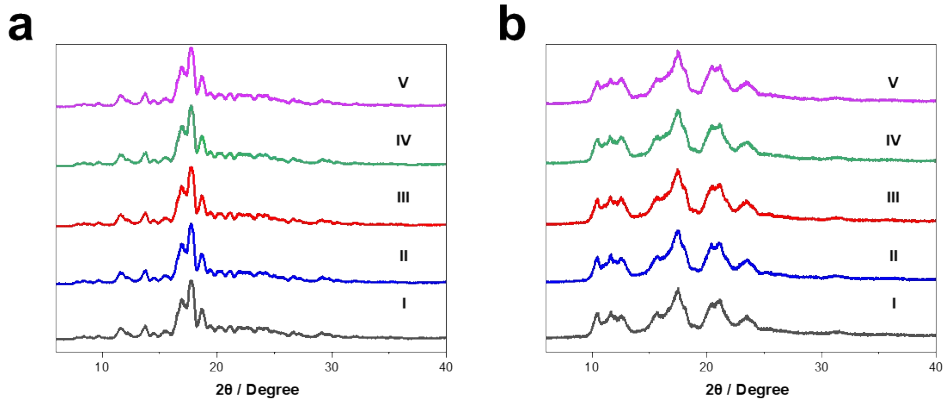

Figure S40. PXRD patterns showing the recyclability of (a) **TI** and (b) **TA** for the adsorption of mixed **Tol**/**MCH** after five cycles.

Table S3. Tol capacity of various adsorbents.

Adsorbents	**Type**	**Uptake of Toluene 298 K and 1.0 bar (mg/g)**	**Method**	**Ref.**
SRC-3K-700	Activated Carbon	1587 mg/g	Vapor sorption isotherm	S10
Activated bone-char	Activated Carbon	1198 mg/g	Vapor sorption isotherm	S11
LDAC	Activated Carbon	600 mg/g	Vapor sorption isotherm	S12
ZIF-67-PLs	Mofs	138 mg/g	Vapor sorption	S13

			isotherm	
Cu-Mof	Mofs	200 mg/g	Vapor sorption isotherm	S14
MIL-101@GQD-3	Mofs	2680 mg/g	Vapor sorption isotherm	S15
UiO-66(NH2)	Mofs	252 mg/g	Vapor sorption isotherm	S16
SMP	Porous polymer	300 mg/g	Vapor sorption isotherm	S17
PS-PMMA-rGO	Porous polymer	250 mg/g	Vapor sorption isotherm	S18
M-1.3	Ordered porous silica	170 mg/g	Vapor sorption isotherm	S19
TAPM-1	Porous Organic Framework	210 mg/g	Vapor sorption isotherm	S20
EtP5	NACS	324 mg/g	Vapor sorption isotherm	S21
EtP6	NACS	156 mg/g	Vapor sorption isotherm	S21
Thiacalixarene	NACS	84 mg/g	Solid−vapor adsorption	S22
TI	NACS	130 mg/g	Solid−vapor adsorption	This work
TA	NACS	127 mg/g	Solid−vapor adsorption	This work

References:

S1 M. Chadim, et al, *Tetrahedron: Asymmetry*., **2001**, *12*, 127–133.

S2 J. Gawronski, et al. *Chem. Eur. J.* **2006**, *12*, 1807–1817.

S3 SAINT. Bruker AXS. Inc, Madison, Wisconsin, USA, 2014.

S4 SADABS. G. M. Sheldrick, University of Gottingen, Germany, 2008.

S5 G. M. Sheldrick, *Acta Crystallogr.*, **2008**, *A64*, 112-122.

S6 L. J. Barbour, *Supramol. Chem.*, **2001**, *1*,189-191.

S7 M. L. Connolly, *Science*, **1983**, *221*, 709-713.

S8 M. L. Connolly, *J. Mol. Graphics*, **1993**, *11*, 139.

S9 T.F. Willems, et al. *Microporous Mesoporous Mater.*, **2012**, *149*, 134-141.

S10 D. Li, J. Yang, Y. Zhao, H. Yuan, Y. Chen. *J. Clean. Prod.*, **2022**, *337*, 130283.

S11 Y. Yang, C. Sun, B. Lin, Q. Huang. *Chemosphere,* **2020**, *256*, 127054.

S12 D. Saha, N. Mirando, A. Levchenko. *J. Clean. Prod.*, **2018**, *182*, 372.

S13 X. Li, et al. *J. Chem. Eng.*, **2021**, *417*, 129239.

S14 G. Li, et al. *Sep. Purif. Technol*., **2021**, *256*, 117781.

S15 M. S. Alivand, *J. Hazard. Mater.*, **2021**, *416*, 125973.

S16 K. Vellingiri, et al. *J. Chem. Eng*., **2017**, *307*, 1116.

S17 Q. Pujol, et al. *Microporous Mesoporous Mater.*, **2022**, *344*, 112204.

S18 M. R. Krishnan, et al. *Environ. Nanotechnol. Monit. Manag.,* **2023**, *20*, 100860.

S19 S. Hou, et al. *J. Chem. Eng*., **2022**, *435*, 134844.

S20 C. Chen, et al. *Angew. Chem. Int. Ed*., **2022**, *61*, e2022016.

S21 K. Jie, et al. *Angew. Chem. Int. Ed*., **2018**, *57*, 12845.

S22 M. Yamada, et al. *Chem. Commun*., **2023**, *59*, 2604.